Thermophysics and Aeromechanics, *2016*, *Vol. 23*, *No. 2*

DOI: 10.1134/S0869864316020037

Numerical simulations of shock-wave interaction with a boundary layer in the plane supersonic flows with jet injection

A.O. Beketaeva*, Ye.S. Moisseyeva, and A.Zh. Naimanova

Institute of Mathematics and Mathematical Modeling, *Almaty*, *Kazakhstan*

E-mail: azimaras@mail.ru*

(*Received October 15*, *2014*; *in revised form August 28*, *2015*)

A supersonic air flow in a plane channel with a transverse turbulent jet of hydrogen injected through a slot on the bottom wall is simulated. The algorithm for solving the Favre-averaged Navier–Stokes equations for the flow of a perfect multispecies gas on the basis of the WENO scheme is proposed. The main attention is paid to the interaction of the shock-wave structure with the boundary layers on the upper and lower duct walls under the conditions of an internal turbulent flow. Namely, a detailed study of the structure of the flow is done, and separation and mixing depending on the jet slot width are investigated. It is found that in addition to well-known shock-wave structures produced by the interaction of the free stream with the transverse jet and the bow shock interaction with the boundary layers near the walls, an additional system of shock waves and the flow separation arise on the bottom wall downstream at some distance from the jet. The comparison with the experimental data is performed.

Key words: supersonic flow, perfect gas, boundary layer, Navier–Stokes equations, shock wave.

Introduction

In most existing works on the theoretical investigation of the interaction between the jet and oncoming flow in the duct, the jet injection region is considered, and, as a rule, the boundary conditions of symmetry or free stream [1–3] are implemented at the top boundary, which facilitates greatly the solution of problems of such a kind. So the processes of the mixing and kinetics of chemical reactions were computed in the work [1] at a transverse injection of the hydrogen sonic jet into a supersonic airflow with parameters $M_\infty = 4$, $T = 1000$ K, $p = 4$ atm. Some peculiarities of the flow were elucidated, in particular, the existence of zones of reverse flows ahead of the injector and behind it was found. The studies of the work [2] were related to a transverse injection of a gaseous fuel at an angle into a low elongated channel of supersonic combustion. It was shown numerically that the fuel injection at an angle leads to an increase in the efficiency of mixing the fuel with air. The authors of [3] studied the influence of the inclination angle of the jet injection on supersonic mixing of gases. It was found that the larger the angle, the higher the total coefficient of the pressure loss in the jet.

The mechanism of the shock-wave structure formation in the above flow has been described well in literature [1–7]. The schematic of the flow in the injection region is shown in Fig. 1. The bow, oblique, and closing shocks form a λ-shaped structure at their intersection.

The schematic depicts the vortices ahead of the jet, which arise as a result of the primary and secondary flow separations from the wall.

In a number of works, the interaction of the injected jet with the shock wave generated from the upper duct wall has been considered, which also simplifies to some extent the problem statement, but enables a detailed study of their interaction. So, the influence of the sizes and location of the generator of a shock wave falling from the top wall on the pressure profiles on the bottom wall in the jet injection region was studied numerically in the work [8]. The generator inclination angle was varied from 15.784° to 35.974°. The authors have shown that the interaction region both ahead of the jet and behind it depends substantially both on the generator inclination angle and on its size. The results of investigating the influence of shock waves on the region of supersonic combustion of a hydrogen jet have been presented in the work [9]. The influence of the incident shock wave on a turbulent boundary layer was also studied numerically in the work [10].

One should note the works devoted to the investigation of the incident shock wave with a boundary layer [11–12]. We note here that there are practically no studies of the shock-wave interaction with the boundary layer under the conditions of the internal turbulent flow. The schematic pattern of the shock-wave interaction with the boundary layer on the duct upper wall is also presented in Fig. 1. It is seen that when the bow shock *1* reaches the top boundary it creates a positive pressure gradient, which proves sufficient for the boundary layer separation on the upper wall. The supersonic region of the boundary layer deflects and gives rise to the compression wave *4* which propagates in the form of the reflected shock *5*. In the work [11], the main attention was paid to the investigation of the structure of the shock-wave interaction with the boundary layer, the separated zone sizes and the dynamic and thermal loads realizing at a reduction or increase of the interaction intensity. The conditions were studied in the work [12], under which the shock-wave inclination angle and strength lead to the boundary layer separation.

Practical interest in the supersonic flow with the injection of jets in a duct is related to the loads both on the upper and lower duct walls. It is obvious that the interaction structure will

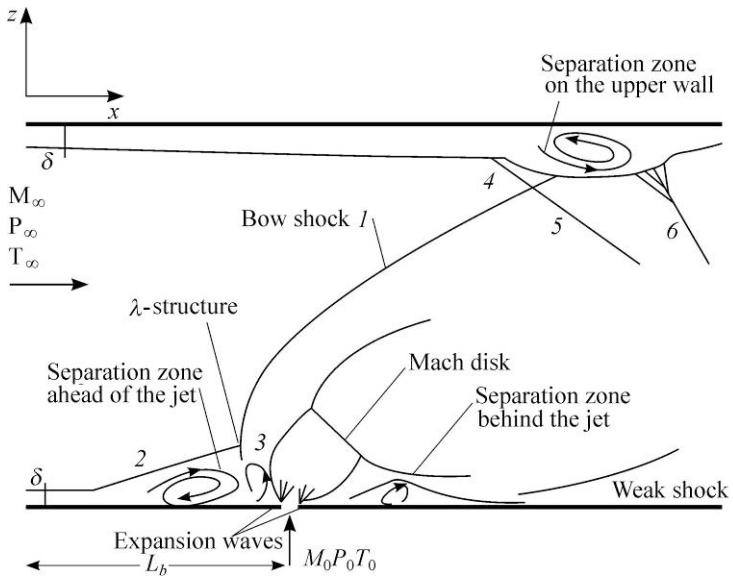

Fig. 1. Flow schematic.

1 — bow shock arising because of the freestream deceleration ahead of the jet,
2 and *3* — the oblique and closing shocks, respectively, *4* — compression wave, *5* — reflected shock,
6 — compression wave arising in the location of the separated flow reattachment.

depend substantially on the injected jet parameters as well as on the height of the duct itself. At present, as was mentioned above, the problems of the shock-wave interaction with the injected jet and with the boundary layers are considered mainly separately. This is related not only to the difficulty of the numerical realization of a complex character of the flow and many species in the gas under consideration but also to the presence of the upper wall, which requires reliable numerical methods.

The purpose of the present work is the numerical simulation of a supersonic flow in a plane duct with a transverse injection of a multispecies jet and the investigation of the interaction of a shock-wave arising upstream of the injected jet with boundary layers both on the bottom and top walls as well as the numerical investigation of the conditions for the boundary-layer separation on the walls and the influence of the jet width on the separation rise.

1. Problem statement

A supersonic airflow with a transverse jet injection from the bottom wall of a rectangular duct (Fig. 1) is considered. The system of the two-dimensional Favre-averaged Navier–Stokes equations for a multispecies gaseous mixture is represented in Cartesian coordinates in the conservative form as

$$\frac{\partial \vec{U}}{\partial t}+\frac{\partial\left(\vec{E}\cdot\vec{E}_v\right)}{\partial x}+\frac{\partial\left(\vec{F}\cdot\vec{F}_v\right)}{\partial z}=0, \tag{1}$$

$$\vec{U}=\left(\rho,\, \rho u,\, \rho w,\, E_{\mathrm{t}},\, \rho Y_k\right)^{\mathrm{T}},$$

$$\vec{E}=\left(\rho u,\, \rho u^2+P,\, \rho uw,\, \left(E_{\mathrm{t}}+P\right)u,\, \rho uY_k\right)^{\mathrm{T}},\quad \vec{F}=\left(\rho w,\, \rho uw,\, \rho w^2+P,\, \left(E_{\mathrm{t}}+P\right)w,\, \rho wY_k\right)^{\mathrm{T}},$$

$$\vec{E}_v=\left(0,\tau_{xx},\tau_{xz},u\tau_{xx}+w\tau_{xz}-q_x,J_{kx}\right)^{\mathrm{T}},\quad \vec{F}_v=\left(0,\tau_{xz},\tau_{zz},u\tau_{xz}+w\tau_{zz}-q_z,J_{kz}\right)^{\mathrm{T}},$$

$$P=\frac{\rho T}{\gamma_\infty \mathrm{M}_\infty^2 W},\quad W=\left(\sum_{k=1}^{N_p}\frac{Y_k}{W_k}\right)^{-1},\quad \sum_{k=1}^{N_p}Y_k=1. \tag{2}$$

$$E_{\mathrm{t}}=\frac{\rho}{\gamma_\infty \mathrm{M}_\infty^2}h-P+\frac{1}{2}\rho\left(u^2+w^2\right),\quad h=\sum_{k=1}^{N_p}Y_kh_k,\quad h_k=h_k^0+\int_{\mathrm{T}_0}^{\mathrm{T}}c_{pk}dT,\quad c_{pk}=C_{pk}/W_k. \tag{3}$$

$$\tau_{xx}=\frac{\mu}{\mathrm{Re}}\left(2u_x-\frac{2}{3}\left(u_x+w_z\right)\right),\quad \tau_{xx}=\frac{\mu}{\mathrm{Re}}\left(2w_z-\frac{2}{3}\left(u_x+w_z\right)\right),\quad \tau_{xz}=\tau_{zx}=\frac{\mu}{\mathrm{Re}}\left(u_z+w_x\right),$$

$$q_x=\left(\frac{\mu}{\mathrm{PrRe}}\right)\frac{\partial T}{\partial x}+\frac{1}{\gamma_\infty \mathrm{M}_\infty^2}\sum_{k=1}^{N_p}h_kJ_{xk},\quad q_z=\left(\frac{\mu}{\mathrm{PrRe}}\right)\frac{\partial T}{\partial z}+\frac{1}{\gamma_\infty \mathrm{M}_\infty^2}\sum_{k=1}^{N_p}h_kJ_{zk},$$

$$J_{kx}=\frac{\mu}{\mathrm{ScRe}}\cdot\frac{\partial Y_k}{\partial x},\quad J_{kz}=-\frac{\mu}{\mathrm{ScRe}}\cdot\frac{\partial Y_k}{\partial z}.$$

The system of equations (1) is written in dimensionless form using conventional notation. The reference flow parameters are $u_\infty, \rho_\infty, T_\infty$, the reference values for the pressure P and the total energy E_{t} are $\rho_\infty u_\infty^2$, the reference values for the specific enthalpy h_k and for the molar specific heats C_{pk} are R^0T_∞/W_∞ and R^0, respectively, the duct height is the reference length, the subscript "∞" refers to freestream parameters; Y_k is the mass concentration of the kth component, the mass concentration index $k=1$ corresponds to O_2, $k=2$ corresponds to H_2 (or He), $k=3$

corresponds to N_2; $N_p = 3$ is the number of species in a mixture of gases, W_k is the molecular weight of the *k*th species, Re, Pr, M, and Sc are the Reynolds, Prandtl, Mach, and Schmidt numbers, respectively, $\tau_{xx}, \tau_{zz}, \tau_{xz}, \tau_{zx}$ are the tensors of viscous stresses, q_x, q_z, J_{xk}, J_{zk} are the thermal and diffusion fluxes (diffusion fluxes are computed by the Fick law), $\mu = \mu_l + \mu_t$ are the coefficients of the laminar and turbulent viscosity. The *k*-ω turbulence model is used for determining μ_t.

2. Boundary conditions

The boundary conditions at the inlet have the following form: $W_k = W_{k\infty}$, $P = P_\infty$, $T = T_\infty$, $u = \mathrm{M}_\infty \sqrt{\dfrac{\gamma_\infty R_0 T_\infty}{W_\infty}}$, $w = 0$, $Y_k = Y_{k\infty}$, $x = 0$, $0 \le z \le H$.

A boundary layer is specified in the inlet section near the duct walls, where the streamwise velocity component is written as $u = 0.1(z/\delta_2) + 0.9(z/\delta_2)^2$ for $x = 0$, $0 \le z \le \delta_2$ and $u = (z/\delta_1)^{1/7}$ for $x = 0$, $\delta_2 \le z \le \delta_1$, here $\delta_1 = 0.37x(\mathrm{Re})^{0.2}$ is the boundary layer thickness, $\delta_2 = 0.1\,\delta_1$ is the near-wall layer thickness (10 % of the boundary layer). The temperature and density values take the form $T = T_\mathrm{w} + u(1 - T_\mathrm{w})$, $\rho = 1/T$, where $T_\mathrm{w} = \left(1 + (r(\gamma - 1)/2)\mathrm{M}_\infty^2\right)$ is the temperature on the wall, $r = 0.88$.

The boundary conditions on the slot have the form $W_k = W_{k0}$, $P = nP_\infty$, $T = T_0$, $w = \mathrm{M}_0 \sqrt{\dfrac{\gamma_0 R_0 T_0}{W_0}}$, $u = 0$, $Y_k = Y_{k0}$, $z = 0$, $L_b \le x \le L_b + h$, where $n = P_0/P_\infty$ is the pressure ratio, subscript "0" refers to the jet parameters. The no-slip and thermal insulation conditions are specified on the bottom and top walls, and the non-reflection conditions are specified at the outlet boundary [13].

3. Solution method

The grid refinement is introduced on the bottom and top walls in the boundary layers as well as at the slot level for a more accurate numerical solution. The system of equations (1) has the following form in the transformed coordinate system:

$$\frac{\partial \tilde{U}}{\partial t} + \frac{\partial \tilde{E}}{\partial \xi} + \frac{\partial \tilde{F}}{\partial \eta} = \frac{\partial \tilde{E}_{v2}}{\partial \xi} + \frac{\partial \tilde{E}_{vm}}{\partial \xi} + \frac{\partial \tilde{F}_{v2}}{\partial \eta} + \frac{\partial \tilde{F}_{vm}}{\partial \eta}, \tag{4}$$

where $\tilde{U} = \vec{U}/J$, $\tilde{E} = \xi_x \vec{F}/J$, $\tilde{F} = \eta_z \vec{F}/J$, $\tilde{E}_{v2} = \xi_x \vec{E}_{v2}/J$, $\tilde{E}_{vm} = \xi_x \vec{E}_{vm}/J$, $\tilde{F}_{v2} = \eta_z \vec{F}_{v2}/J$, $\tilde{F}_{vm} = \eta_z \vec{F}_{vm}/J$, $J = \partial(\xi, \eta)/\partial(x, z)$ is the transformation Jacobian. The parameters of the coordinate transformation are described in detail in the works [17, 18].

At present, the quasi-monotone conservative schemes of higher approximation order are widely applied for the solution of such complex problems. These are such schemes as TVD (Total Variation Diminishing Schemes), ENO (Essentially Nonoscillatory Schemes), and WENO (Weighted ENO) [14–19].

In this work, the convective terms are approximated by using the WENO scheme the idea of the construction of which is based on the ENO scheme presented in the works [17, 18].

The temperature field is calculated from the known values of the original variables with the use of the equation

$$f(T) = E_t - \frac{\rho}{\gamma_\infty \mathrm{M}_\infty^2 W}\left(\tilde{H}(T) - RT\right) - \frac{1}{2}\rho\left(u^2 + w^2\right) = 0, \tag{5}$$

where $\tilde{H}$ is the molar enthalpy of the mixture of the gases. The solution of the algebraic equation (5) with respect to the temperature is found by the Newton–Raphson iteration method possessing the quadratic convergence rate [17, 18].

4. Results of computations and their analysis

Test problem 1

For a comparison with the experimental data the computation of the plane supersonic airflow has been done ($\mathrm{M}_\infty = 2.9$, $P_\infty = 0.0663$ MPa, $T_\infty = 108$ K) with the perpendicular injection of the helium sonic jet ($T_0 = 217$ K, $P_0 = 1.24$ MPa) through a slot of width 0.0559 cm on the bottom wall. The height H and the width L of the duct are 7.62 and 25 cm, respectively. The specific heats at constant pressure of the kth species C_{pk} are computed with the use of the polynomial fourth-order interpolation in temperature:

$$C_{pk} = \sum_{i=1}^{5} a_{ki} T^{i-1}, \tag{6}$$

where $\{a_{ki}\}$ are the empirical constants. The experimental data of the work [20] are used here for determining the $\{a_{ki}\}$ at a temperature below 300 K (see the Table). For the temperature within $300 < T < 5000$ K, the values of empirical constants are taken from the work [21].

To estimate the accuracy of the difference scheme and its efficiency the computations of the pressure distribution on the wall ahead of the slot and behind it were done on a sequence of grids with the number of grid nodes from 301×221 to 421×281. The pressure distributions on the wall, which were computed on the different grids, are shown in Fig. 2. An increase of the number of the computational grid nodes leads to that the experimental results and computed curves practically coincide starting from the nodes number 381×281 and higher, and one can see in the figure a good agreement between the numerical and experimental data. Thus, one can speak about a sufficient accuracy of the scheme for the grids with nodes number 381×281 and higher, which enables the problem solution on the grids of these sizes.

Table

The values of empirical constants $\{a_{ki}\}$

$T < 300$	O_2	N_2	He
a_{k1}	$0.34843577 \cdot 10^{2}$	$0.39755287 \cdot 10^{2}$	$0.209336046 \cdot 10^{2}$
a_{k2}	$-0.90674514 \cdot 10^{-1}$	$-0.20027529 \cdot 10$	$0.000000000 \cdot 10$
a_{k3}	$0.56072001 \cdot 10^{-3}$	$0.14293081 \cdot 10^{-2}$	$0.000000000 \cdot 10$
a_{k4}	$-0.15761941 \cdot 10^{-5}$	$-0.45017727 \cdot 10^{-5}$	$0.000000000 \cdot 10$
a_{k5}	$0.17168133 \cdot 10^{-8}$	$0.52356848 \cdot 10^{-8}$	$0.000000000 \cdot 10$

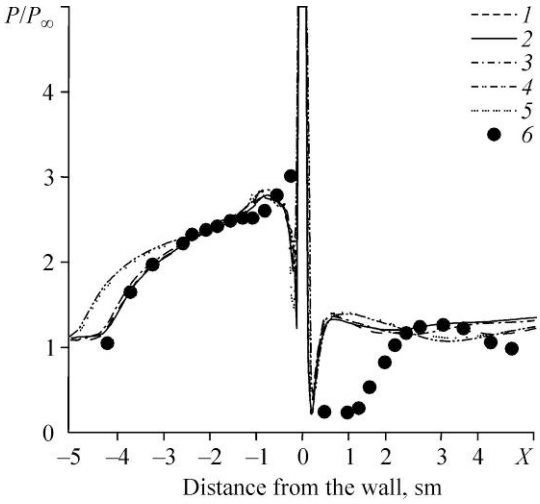

Fig. 2. Pressure distribution on the wall.
The number of grid nodes: 421×281 (*1*), 401×281 (*2*), 381×281 (*3*), 301×281 (*4*), 301×221 (*5*), experimental data of the work [1] (*6*); M_∞ = 2.9, P_∞ = = 0.0663 MPa, T_∞ = 108 K, T_0 = 217 K, P_0 = 1.24 MPa.

Test problem 2

The next test problem is the modeling of the incident shock wave with a turbulent boundary layer. The supersonic flow along a thin plate with a shock generator on the upper boundary is considered with the parameters corresponding to the experiments [12], where the freestream Mach number $M_\infty = 5$, the Reynolds number $Re = 40 \cdot 10^6$, the wall temperature $T_w = 300$ K. The computations were done for the shock-generator angle $\alpha = 14°$ which corresponds to the separated flow of the boundary layer. Figure 3 shows the computed results of the present work and the data of [12] on friction coefficients (Fig. 3*a*) and the pressure (Fig. 3*b*) on the wall. An insignificant discrepancy in the region of the shock-wave falling onto the wall (it corresponds in Fig. 3*b* to the region of a rapid pressure increase on the wall) is obviously explained by that in the work [12] the system of the Navier–Stokes equations for a single-component perfect gas is used, whereas in the present work, the system of the equations for a multispecies gas is employed, where it is necessary to solve iteratively equation (5) to determine the temperature. One can note, on the whole, a satisfactory agreement between experiments and computations.

Investigation of the jet width effect

The results of the computations of the problem (1), where the sizes (h_1, h_2, h_3) of the slot for the injected jet are varied, are presented below in Figs. 4–6. The dimensionless parameters of the computational region have the following values: the duct length $L = 6.25$,

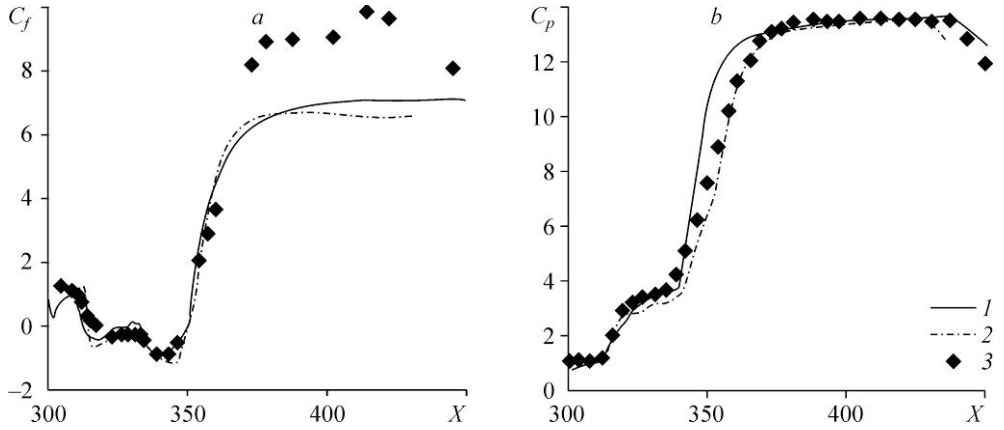

Fig. 3. Distribution of the friction coefficient (*a*) and pressure (*b*) on the wall.
Computations: *1* — WENO scheme, *2* — results of the work [12]; *3* — experimental data of the work [12].

the height $H = 1$. In the first case, the duct width size $h_1 = 0.05$, in the second case, $h_2 = 0.066$, and in the third case, $h_3 = 0.083$. At the numerical computation, the boundary layer thickness $\delta_1 = 0.1$, which has been computed for $x = 12$, is specified at the inlet section. The near-wall layer height then corresponds to the laminar-turbulent sublayer $z^+ = 70$, where $z^+ = \delta_2 u_\tau / \nu$, and the boundary layer height is $z^+ = 3700$, where $z^+ = \delta_1 u_\tau / \nu$. Here $u_\tau = \left(0.5 C_\mathrm{f}\right)^{1/2}$ is the dynamic viscosity, C_f is the flow friction coefficient on the wall. The grid is refined near the wall in such a way that the condition $z^+ = 1.5$ is satisfied for the first grid node near to the wall, 5–8 nodes lie in the near-wall layer along the *z*-axis, and the entire boundary layer is calculated with the use of 35–40 nodes of the numerical grid.

The freestream parameters are as follows: $\mathrm{M}_\infty = 3.75$, $T_\infty = 629.43$ K, $\mathrm{Re} = 10^6$, $\mathrm{Pr} = 0.7$; the jet temperature $T_0 = 800$ K, the pressure ratio *n* is equal to 15. The data of numerical experiments on the interaction of shocks with the boundary layers for the slots of the different width are shown in Fig. 4. As a result of the jet interaction with free stream, the formation of the systems of shocks, which correspond to the ones studied previously and are shown schematically in Fig. 1, is observed. Due to a freestream deceleration ahead of the injected jet, the bow shock *1* arises, from which the oblique shock *2* departs upstream. There are behind the oblique shock the regions of supersonic zones the deceleration of which is followed by the appearance of the closing shock *3*. The detached bow, oblique, and closing shocks are seen to form a λ-shaped system. As follows from Fig. 4*c*, for h_3, shock *3* is expressed weakly, whereas for the other two cases (Figs. 4*a* and 4*b*) it is clearly seen.

It follows from Fig. 4 that when the bow shock *1* reaches the upper boundary it creates a positive pressure gradient, which proves sufficient for the boundary layer separation on the upper wall. The supersonic region of the boundary layer then deviates and gives rise to compression wave *4*, which propagates in the form of the reflected shock *5*. Also, from the graphs, a fan of the expansion waves in the boundary layer can be seen in the form of the shadows behind shock 5, which are due to the flow expansion in the region behind shock *1*. Thus, a pattern of the shock-wave interaction with the boundary layer, which is well known in the literature, is observed here. As a result of the separated flow reattachment

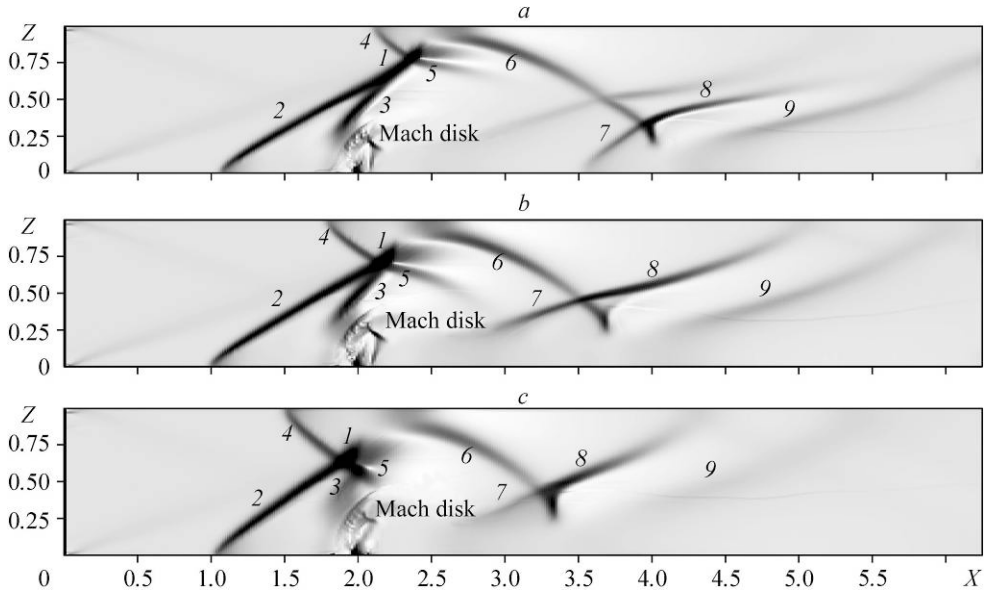

Fig. 4. Distribution of isobars for the slots of different widths.
h_1 (*a*), h_2 (*b*), h_3 (*c*); $T_0 = 800$ K, $\mathrm{M}_\infty = 3.75$, $T_\infty = 629.43$ K, $\mathrm{Re} = 10^6$, $\mathrm{Pr} = 0.7$.

to the streamlined wall, the reflected shock *6* arises downstream in the region of the mixing of the separated boundary layer with external flow, where the flow again becomes non-separated.

Similarly to the pattern ahead of the jet, the bow shock *1*, the compression wave *4*, and the reflected shock *5*, which intersect at a single point, form a λ-shaped system. The sizes of this λ-shaped structure increase considerably with increasing the slot width, and this can be observed by comparing Figs. 4*a*–4*c*. The jet width increase is seen to lead to that the compression wave *4*, which has formed near the upper wall, shifts significantly towards the inlet boundary.

The Mach disk can be clearly seen in the graphs of isobars *4*. An increase in the slot sizes leads to enlargement of the barrel structure in the jet and, as a consequence, to a Mach disk increase (Figs. 4*a* and 4*b*). However, in the case of the maximum slot size (h_3) (Fig. 4*c*), the Mach disk decreases because the separation zone shifts towards the inlet boundary. Respectively, the distance between the jet and the upper reverse region becomes minimal (confuser), due to which the free stream accelerates considerably thereby impeding the jet expansion.

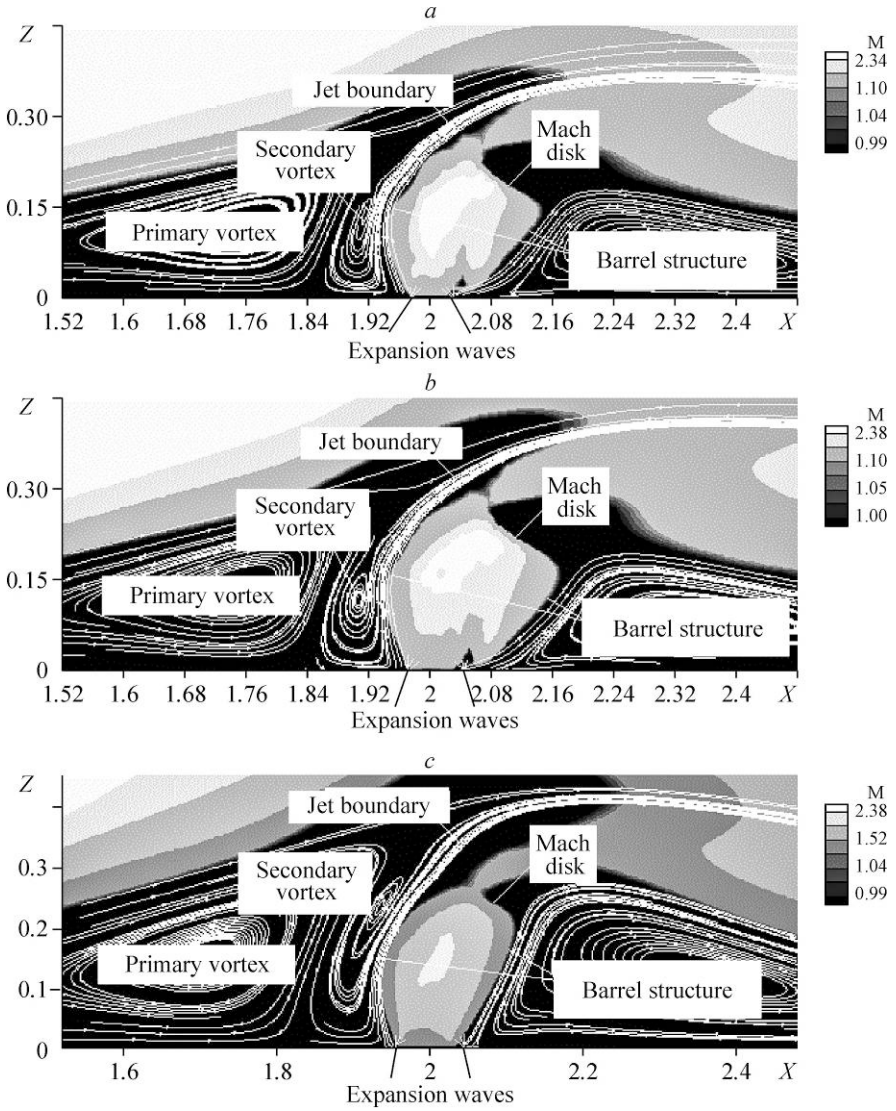

Fig. 5. Local Mach number distribution for the slots of different widths.
h_1 (*a*), h_2 (*b*), h_3 (*c*); T_0 = 800 K, M_∞ = 3.75, T_∞ = 629.43 K, Re = 10^6, Pr = 0.7.

It follows from Fig. 4 that besides the well-known shock-wave pattern an additional structure arises, which is due to the interaction of the reflected shock *6* with the boundary layer on the lower wall behind the jet. The interaction between the bottom boundary layer and shock *6* is seen to be similar to a pattern observed on the upper wall that is compression wave *7* is created, which propagates in the form of shock *8*. The weak reflected shock *9* is also can be seen here.

It is known that at the exhaustion of an underexpanded jet into the flow the pressure in the jet tends to become equal to the ambient medium pressure. As a consequence of this, the jet expansion occurs with the formation of a family of the expansion waves which move towards the jet boundaries and form the barrel shock closed by the Mach disk, which is demonstrated by the distribution of the local Mach number ($\mathrm{M} = \sqrt{u^2 + w^2}/c$, here c is the local sound speed) shown in Fig. 5. Figures 5*a* and 5*b* show a growth of the barrel sizes with increasing slot width. However, in accordance with the above-said about the pressure distribution (see Fig. 4), from the Mach number contours for h_3 (Fig. 5*c*) a narrowing of the barrel can be observed despite the fact that the slot width is maximal.

The results of numerical experiments for the velocity vector field shown in Fig. 6 demonstrate the vortex structure pattern. It is seen from the graph that for all cases under consideration, two vortices form in a zone adhering to the wall ahead of the jet. The motion directions in these

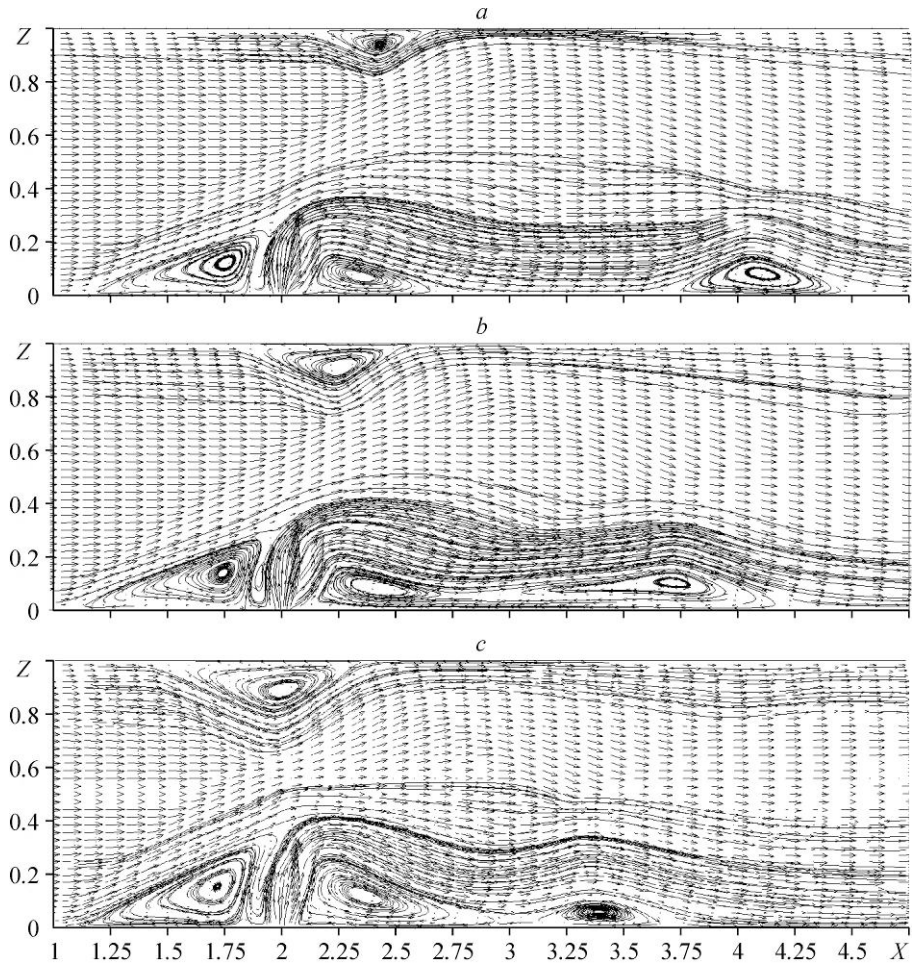

Fig. 6. Distribution of the velocity vector field for the slots of different widths.
h_1 (*a*), h_2 (*b*), h_3 (*c*); T_0 = 800 K, M_∞ = 3.75, T_∞ = 629.43 K, Re = 10^6, Pr = 0.7.

vortices are opposite because part of the airflow in a direct proximity of the wall passing through the regions of the oblique (*2*) and closing (*3*) shocks turns downwards to the wall and penetrates the separated flow zone, and then diverges in opposite directions. The rise of a vortex region behind the jet is due to a zone of the low pressure. One can also see in the graphs a separation region on the upper wall because of the bow shock *1* interaction with the upper boundary layer. The qualitative patterns of reverse zone are similar in all three cases; however, they differ quantitatively because the sizes of the boundary layer separation at the upper wall increase substantially with the slot width growth.

Figures 6*a*–6*c* highlight an additional vortex besides the known ones on the bottom wall at some distance behind the jet, which has formed as a result of the interaction of the shock *6* with the lower boundary layer. As follows from the graphs, its shift towards the jet takes place with increasing slot sizes (cf. Figs. 6*a*–6*c*). Thus, the growth of the slot sizes leads to the increase in the air and fuel mixing directly behind the injected jet because of the vast zones of the reverse flows.

Conclusions

The shock-wave structure and the separation region arising because of the interaction of the shocks with the boundary layers both on the top and bottom duct walls have been studied in dependence of the injected jet sizes with the use of numerical experiments. The reduction of the jet expansion with the slot width increase, which is a consequence of the confuser rise between the injected jet and the separation zone on the upper wall, is shown. It is found that besides the well-known shock-wave pattern, there arises here an additional structure due to the interaction of the reflected shock *6* with the boundary layer on the bottom wall at some distance behind the jet, which may lead to an increase in the air and fuel mixing due to large zones of reverse flows. A comparison of computations with the experimental data shows a satisfactory agreement of the results.

References

1. **J.S. Shuen and S. Yoon,** Numerical study of chemically reacting flows using an LU-SSOR scheme, AIAA J., 1989, Vol. 27, P. 1752–1760.
2. **F.C. Chenault and P.S. Beran,** k-ε and Reynolds stress turbulence model comparisons for two-dimensional injection flows, AIAA J., 1998, Vol. 36, No. 8, P. 1401–1412.
3. **S. Aso, K. Inoue, K. Yamaguchi, and Y. Tani,** A study on supersonic mixing de circular nozzle with various injection angles for air breathing engine, Acta Astronautica, 2009, Vol. 65, Nos. 5, 6, P. 687–695.
4. **F.W. Spaid and E.E. Zukoski,** A study of the interaction of gaseous jets from transverse slots with supersonic external flows, AIAA J., 1968, Vol. 6, No. 2, P. 205–212.
5. **V.S. Avduevskii, K.I. Medvedev, and M.N. Polyanskii,** Interaction of a supersonic flow with a transverse jet injected through a circular aperture in a plate, Fluid Dyn., 1970, Vol. 5, No. 5, P. 888–891.
6. **A.I. Glagolev, A.I. Zubkov, and Yu.A. Panov,** Interaction between a supersonic flow and gas issuing from a hole in a plate, Fluid Dyn., 1968, Vol. 3, No. 2, P. 65–67.
7. **J.A. Schetz, P.F. Hawkins, and H. Lehman**, Structure of highly underexpanded transverse jets in a supersonic stream, AIAA J., 1967, Vol. 5, No. 5, P. 882–884.
8. **W. Huang, Z. Wang, J. Wu, and Sh. Li,** Numerical prediction on the interaction between the incident shock wave and the transverse slot injection in supersonic flows, Aerospace Science and Technology, 2012, Vol. 28, No. 1, P. 1–9.
9. **J.H. Kim, Y. Yoon, I.S. Jeung, H. Huh, and J.Y. Choi,** Numerical study of mixing enhancement by shock waves in model scramjet engine, AIAA J., 2003, Vol. 41, No. 6, P. 1074–1080.
10. **W.W. Liou, G. Huang, and T.H. Shih,** Turbulence model assessment for shock-wave/turbulent boundary-layer interaction in transonic and supersonic flows, Computers and Fluids, 2000, No. 29, P. 275–299.
11. **D. Knight, H. Yan, A. Panaras, and A. Zheltovodov,** RTO WG 10: CFD validation for shock-wave turbulent boundary layer interactions, AIAA Paper, 2002, No. 2002–0437.
12. **N.N. Fedorova and I.A. Fedorchenko,** Computations of interaction of an incident oblique shock wave with a turbulent boundary layer on a flat plate, J. Appl. Mech. Tech. Phys., 2004, Vol. 45, No. 3, P. 358–366.

13. T.J. Poinsot and S.K. Lele, Boundary conditions for direct simulation of compressible viscous flows, J. Comput. Phys., 1992, Vol. 101, P. 104–129.
14. A. Harten, S. Osher, B. Engquist, and S.R. Chakravarthy, Some results on uniformly high-order accurate essentially non-oscillatory schemes, Applied Num. Math., 1986, No. 2, P. 347–377.
15. S.V. Ershov, A quasi-monotone higher-order ENO scheme for integrating the Euler and Navier–Stokes equations, Matematicheskoe modelirpovanie, 1994, Vol. 6, No. 11, P. 63–75.
16. J.Y. Yang, Third-order non-oscillatory schemes for the Euler equations, AIAA J., 1991, Vol. 29, No. 10, P. 1611–1618.
17. A.O. Beketaeva and A.Zh. Naimanova, Application of ENO (essentially nonoscillatory) scheme to modeling of multi-component flows, Computational Technologies, 2007, Vol. 12, Special issue 4, P. 17-25.
18. P. Bruel and A.Zh. Naimanova, Computation of the normal injection of a hydrogen jet into a supersonic air flow Thermophysics and Aeromechanics, 2010, Vol. 17, No. 4, P. 531–541.
19. X. Liu, S. Osher, and T. Chan, Weighted essentially non-oscillatory schemes, J. Comput. Phys., 1994, Vol. 115, P. 200–212.
20. The Tables of Physical Quantities, Handbook**,** I.K. Kikoine (Ed.), Atomizdat, Moscow, 1976.
21. R.J. Kee, F.M. Rupley, and J.A. Miller, CHEMKIN-II: a fortran chemical kinetic package for the analysis of gas-phase chemical kinetics, Sandia Report SAND89-8009B, Sandia National Laboratories, Albuquerque, 1989.